Cooperative effects of tropical Pacific and Atlantic SST forcing in southern China winter precipitation variability

Yunyun Liu[1,2] · Zeng-Zhen Hu[3] · Renguang Wu[4]

Abstract

This study investigates the variability of winter precipitation over southern China (SC) and the impacts of sea surface temperature (SST) forcing in the tropical Pacific and Atlantic Oceans. The SC winter precipitation displays two major spatial modes: a same-sign mode with the maximum center located in southeastern China, and a north–south dipole mode with opposite variations between the lower reach of the Yangtze River and the southeastern coast of China. Both modes are associated with the variation of the western North Pacific (WNP) anticyclone. The same-sign mode is associated with canonical El Niño through the Pacific-East Asian teleconnection in the lower troposphere. The north–south dipole mode is subject to the impact of the western Pacific warm pool associated with the central Pacific El Niño and equatorial Atlantic forcing. The influence of equatorial Atlantic warming is through an upper-tropospheric zonal wave pattern from the tropical Atlantic to the mid-latitudes of East Asia. Both the tropical Pacific and Atlantic oceanic forcing induce a north–south dipole pattern of winter precipitation anomalies over SC by affecting the northward extension of the WNP anticyclone. Moreover, the observed statistical relationship between the dipole mode and the equatorial Atlantic SST anomalies is present in hindcasts/ forecasts of the NCEP Climate Forecast System version 2 (CFSv2), confirming a potential source of the predictability of the north–south dipole-like variation of the winter precipitation in SC.

Keywords Winter precipitation over southern china · Same-sign mode · North–south dipole mode · ENSO · Equatorial atlantic warming · Predictability

1 Introduction

Southern China (SC) is a climate-sensitive region due to the large population and active economic flow. Also, the precipitation in this region presents an obvious interannual variability in both summer and winter. The precipitation-related climate extreme events have resulted in huge economic and social damage. Previous studies indicated that the interannual variability of precipitation in China is partially driven by the oceanic forcing, and the El Niño-Southern Oscillation (ENSO) is considered of paramount importance (Lau and Nath 2003; Wu et al. 2003; Chang et al. 2004; He and Wang 2013; He and Wu 2014; Jang et al. 2016; Jin et al. 2016). Statistically, winter precipitation in SC tends to be above normal during the mature phase of an El Niño event (Zhang et al. 1999; Zhang and Sumi 2002; Wu et al. 2003; Ke et al. 2019), such as the winter 1982/83, 1997/1998, and 2015/16.

In recent years, it was noted that on average, precipitation anomaly in SC is larger during the mature phase of eastern Pacific (EP) El Niño than that of central Pacific (CP) El Niño (Feng et al. 2010; Hu et al. 2012; Yuan and Yang 2012; Xu et al. 2019; Ke et al. 2019). Geographically, compared with EP El Niño, the maximum wet center shifts northward from the southeast coast of SC to the lower reach of the Yangtze River (LRYR) in CP El Niño (Su et al. 2013). The different precipitation distributions over SC in EP and CP El Niño

✉ Yunyun Liu
 liuyuny@cma.gov.cn

[1] National Climate Center, Chinese Meteorological Administration, #46 Zhong-Guan-Cun South Road, Beijing 100081, China

[2] Collaborative Innovation Center On Forecast and Evaluation of Meteorological Disasters, Nanjing University of Information Sciences & Technology, Nanjing 210044, China

[3] Climate Prediction Center, NCEP/NOAA, College Park, MD 20740, USA

[4] School of Earth Sciences, Zhejiang University, Hangzhou 310027, Zhejiang, China

are attributed to differences in anomalous Walker circulation and low-level anticyclone around the Philippines (Feng et al. 2010).

In addition to the effects of ENSO, the winter precipitation anomalies in SC may be affected by other external forcings, such as sea surface temperature anomalies (SSTAs) in the tropical western Indian Ocean (Liu et al. 2010), in the North Atlantic Ocean (Li and Bates, 2007; Fu et al. 2008; Han et al. 2011), in the tropical Atlantic Ocean (Chen et al. 2015; Liu et al. 2020), in the Kuroshio Sea (Zong et al. 2008; Liu et al. 2010), as well as convective activities in the equatorial central and western Pacific Ocean (Nitta and Hu 1996; Guo and Ni 1998). These external forcings affect the precipitation anomalies in SC through modifying the geopotential height and wind fields in the upper and lower troposphere over the Asian region (Zhang et al. 2008; Liu et al. 2013).

In winter 2018/19, precipitation was 100–200 mm above the climate mean in LRYR, greater than two standard deviations, associated with a weak CP or CP/EP mixed type El Niño (Ren and Jin 2011; Guo et al. 2019; Liu et al. 2020). On the other hand, the excessive precipitation did not occur in the entire SC, and there was deficit precipitation in the southeastern coast of SC (Liu et al. 2020). Thus, it was a dipole-like pattern in SC with positive precipitation anomaly in the north and negative anomaly in the south. It seems difficult to explain the extremely wet winter 2018/2019 simply with the previously identified impacts of EP El Niño or CP El Niño. So, what caused the abundant precipitation over LRYR or the dipole-like variation of the precipitation in winter 2018/19? What are the leading patterns of winter precipitation in SC and their associated oceanic forcing? To answer these questions, after isolating the leading patterns of the winter precipitation in SC, the associated atmospheric circulation patterns in both the upper and lower troposphere and the roles of tropical SSTAs will be analyzed in this work. Our purpose is to have a better understanding of the variability and predictability of the winter precipitation anomalies in SC.

2 Datasets, SSTA indices, and model

The datasets in this work include precipitation of 753 stations in China provided by the China Meteorological Administration, NOAA's PRECipitation REConstruction Dataset (Chen et al. 2002), and the US National Centers for Environmental Prediction/National Center for Atmospheric Research (NCEP/NCAR) reanalysis products (Kalnay et al. 1996), including monthly and daily mean geopotential height, specific humidity, horizontal winds, stream function, and surface pressure. The vertically integrated water vapor transport (Q) is defined as follows:

$$Q = -\frac{1}{g}\int_{p_s}^{p} qU dp$$

Here, g is the acceleration due to gravity. q is special humidity, and U is a horizontal wind vector. p_s represents surface pressure, and p stands for the top pressure, which is chosen as 300 hPa. The divergences (D) is calculated using.

$D = \frac{\partial Q_u}{a\cos\varphi\,\partial\lambda} + \frac{\partial Q_v}{a\,\partial\varphi}$, where a is the earth radius, φ and λ represent the latitude and longitude, respectively. The unit of D is kg m^{-2} s^{-1}.

This study focuses on the winter (DJF) season covering the 1981/82–2018/19 period. Anomalies of all variables are defined as the deviations from the climatological mean of DJF for the period 1981/82–2010/11. Linear correlation and regression, composite, and empirical orthogonal function (EOF) analysis are used in this study based on seasonal mean anomalies. The statistical significance of the correlation is estimated based on the two-tailed Student's t-test. For the winters of 1981/82–2018/19, the correlation coefficients at the confidence levels of 90%, 95%, and 99% are 0.27, 0.32, and 0.41, respectively. The linear trend of all variables including the following SST indices has been removed prior to the correlation and regression analyses to focus on interannual variations (Huo et al. 2015).

Monthly mean SST on a 2°×2° resolution is extracted from the National Oceanic and Atmospheric Administration Extended Reconstructed SST, version 5 (ERSSTv5; Huang et al. 2017). To measure the tropical SSTA variations and their association with the atmosphere and precipitation anomalies, multiple SSTA indices are selected in this work. In addition to the Niño3.4 index, Cold Tongue (CT) and Warm Pool (WP) (Kug et al. 2009; Ren and Jin 2011) and Modoki (Ashok et al. 2007) indices are used to represent different flavors of ENSO. Also, the western Pacific warm pool (NiñoW) index, the Indian Ocean basin mode (IOBM, Chambers et al. 1999), and the equatorial Atlantic Niño (ATL3, Zebiak 1993) are selected to represent the tropical SSTA forcing in different ocean basins. The definitions of these SSTA indices are shown in Table 1.

Besides, ensemble means of predictions (hindcasts in 1982–2011 and real-time forecasts since 2012) initiated from January 1982-December 2018 from the NCEP Climate Forecast System version 2 (CFSv2) are examined to investigate the predictability of winter precipitation variability in SC and to verify the statistical connection with SSTAs (Xue et al. 2013; Saha et al. 2014; Hu et al. 2013; 2014; 2017). The ensemble means of model predictions include 28 members each month, out to 9 months. The atmospheric component of CFSv2 has a spectral triangular truncation of 126 waves (T126) in the horizontal and a finite differencing in the vertical with 64 sigma-pressure hybrid layers, while the ocean model has 40 vertical layers

Table 1 The definitions of the selected tropical SST indices

SST index	Definition
Niño3.4	SSTA (5°S–5°N, 170°–120°W)
CT	$SSTA_{Niño3}$ (5°S–5°N, 150°–90°W)—$\alpha*SSTA_{Niño4}$ (5°S–5°N, 160°E–150°W), (while $SSTA_{Niño3}*SSTA_{Niño4} > 0$, $\alpha = 0.4$; otherwise, $\alpha = 0$)
WP	$SSTA_{Niño4}$ (5°S–5°N, 160°E–150°W)—$\alpha*SSTA_{Niño3}$ (5°S–5°N, 150°–90°W), (while $SSTA_{Niño3}*SSTA_{Niño4} > 0$, $\alpha = 0.4$; otherwise, $\alpha = 0$)
Modoki	SSTA (10°S–10°N, 165°–140°W)—[SSTA (15°S–5°N, 110°–70°W) + SSTA (10°S–20°N, 125°–145°E)]/2
NiñoW	SSTA(0°–10°N,120°–140°E)
IOBM	SSTA (20°S–20°N, 40°–110°E)
ATL3	SSTA (3°S–3°N, 20°W–0°)

with the meridional resolution of 1⁄4° between 10°S and 10°N, gradually increasing to 1/2° poleward of 30°S and 30°N (Saha et al. 2014).

3 Different types of SST and atmospheric anomalies influences on the winter precipitation variability over SC

3.1 Leading modes of winter precipitation over SC

Climatologically, precipitation amount in winter generally decreases from south to north over China, and SC has a climate mean precipitation amount of 100–280 mm in DJF (Wu et al. 2003; Ke et al. 2019; Liu et al. 2020). For the spatial variation pattern, Fig. 1 shows the first two EOF modes of the winter precipitation variation in the SC domain and their corresponding Principal Components (PCs) from 1981/82 to 2018/19. The two leading modes are a same-sign SC mode (the 1st mode of EOF, EOF1) with the maximum center located in southeastern China and a south-north dipole mode (the 2nd mode of EOF, EOF2) with the opposite variations between LRYR and the southeastern coast of China, respectively (Fig. 1a, b). The variance contributions of the two modes are 53.6% and 21.2%, respectively. Both PCs show profound interannual variability, and the value of PC2 is the largest in winter 2018/19 (Fig. 1c, d). According to the North's rule of thumb for EOF significance (North et al. 1982), the two leading modes of winter precipitation over SC can be separated from each other.

The relationships between the two leading modes of winter precipitation anomaly over SC and the atmospheric and oceanic variables are discussed in the next two subsections. The simultaneous regressions of the SSTA and atmospheric circulation anomaly onto PCs are conducted to identify the remote forcing associated with the variability of winter precipitation in the SC region.

3.2 Atmospheric and oceanic anomalies associated with the same-sign mode EOF1

Figure 2a presents the simultaneous regressions of the SSTA and atmospheric circulation anomaly onto PC1. Corresponding to positive PC1, the tropical ocean is mainly characterized by warming in the equatorial central and eastern Pacific and cooling in the western Pacific warm pool, featuring a canonical El Niño-like pattern (Wang et al. 2000; Wu et al. 2003). Among the correlations of PC1 with various SST indices shown in Table 2, the most significant one is between PC1 and CT index, confirming that the same-sign mode is mainly associated with the canonical El Niño or EP El Niño. The SSTA and associated atmospheric circulation anomaly patterns are nearly identical to those from regressions with CT index (not shown). Besides, the tropical Indian Ocean also shows moderate basin-wide positive correlations, consisting with the fact that waring (cooling) in the tropical Indian Ocean often occurs accompanying El Niño (La Niña) events, with 1~2 season lag (Chambers et al. 1999; Xie et al. 2009; Wang et al. 2019). The correlation coefficients of IOBM with both Niño3.4 and CT indices are 0.76 (Table 2), consistent with a coherent variation between ENSO and basin-wide Indian Ocean SST.

In response to both the tropical Pacific and Indian oceanic warming, anomalous westerly occurs over the equatorial central-eastern Pacific, and anomalous easterly appears from the warm pool to the eastern Indian Ocean, and twin anomalous anticyclones emerge over the western Pacific, symmetric with respect to the equator to some extent (Fig. 2a). The western North Pacific (WNP) anticyclone includes two separate centers, with a tropical center located over the Philippine Sea, and an extratropical center over the Kuroshio extension, which is consistent with previous studies (e.g., Wang et al., 2000). Anomalous southerlies prevail to the western edge of the anomalous Philippine Sea anticyclone, weakening the East Asian winter monsoon.

The relationship between tropical heating and atmospheric circulation pattern can be used to examining the effect

Fig. 1 **a**, **b** The first two EOF modes and (**c**, **d**) the corresponding principal components (PCs) of winter precipitation anomaly (mm) over South China (SC, [18°–35°N,105°–123°E]) for the period of 1981/82–2018/19
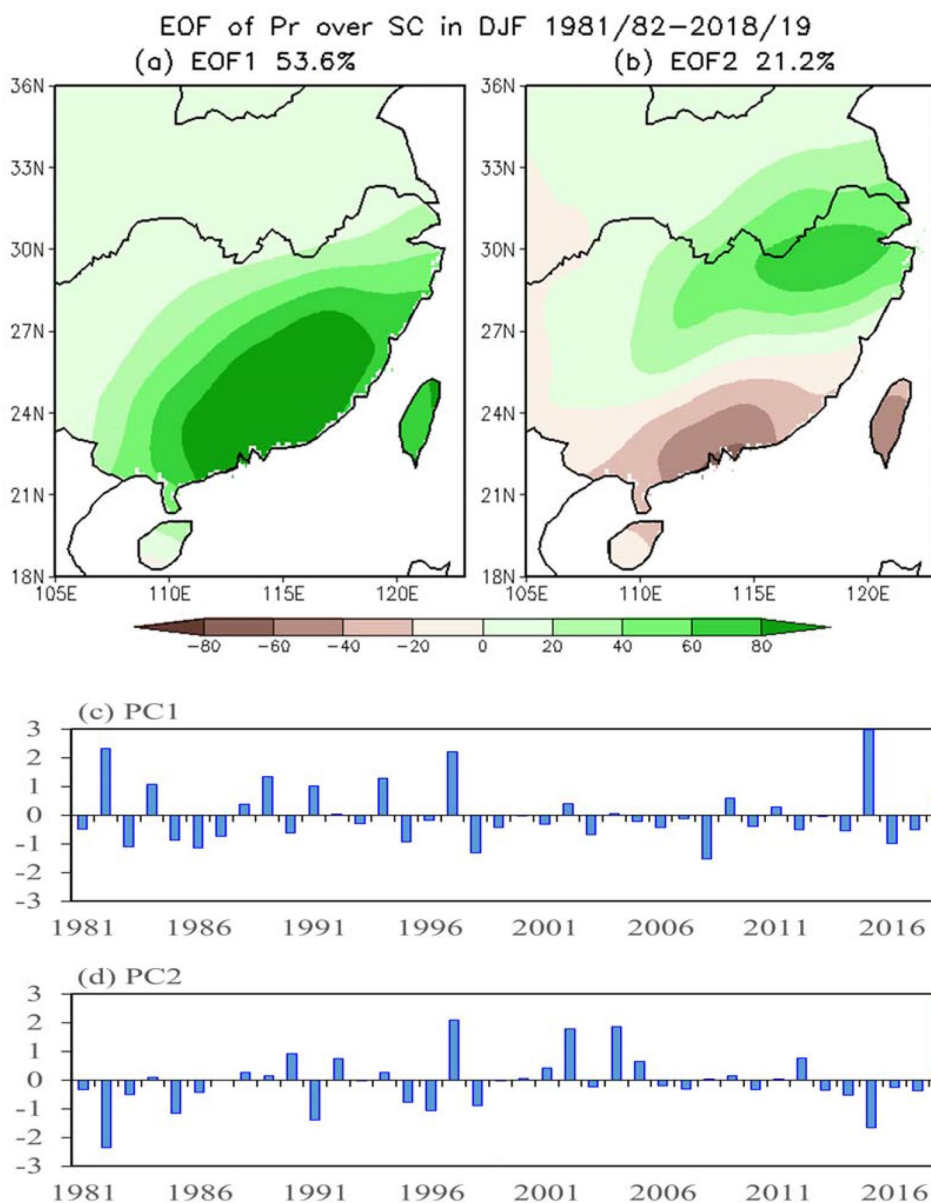
of tropical SST forcing (Peng et al. 2019). Figure 2b presents the regression of DJF precipitation and low-level stream function anomalies onto PC1. The precipitation anomalies in the tropical Pacific have an east–west dipole structure, with above-normal precipitation (heating) east of the Dateline and below-normal (cooling) in the western Pacific. In terms of stream function in the lower troposphere, the antisymmetric anomalous stream function pattern about the equator indicates cyclonic rotational flows forming at both sides of the equator, feature a Rossby wave response to the anomalous heating over the equatorial central-eastern Pacific (Gill 1980; Alexander et al. 2002) associated with the ENSO warming. The northeasterly anomalies reside in the eastern part of the WNP anticyclone and the southwesterly anomalies emerge in the western part of the WNP anticyclone along the coast

of the East Asian continent. Thus, the WNP anticyclone bridges the forcing in the equatorial central-eastern Pacific and the atmospheric circulation anomaly over SC, leading to convergence of moisture and above-normal precipitation in SC (Fig. 4a). It is a typical pattern of the Pacific-East Asian teleconnection referred to by Wang et al. (2000). Furthermore, this teleconnection pattern is primarily confined to the lower troposphere, and it almost disappears in the upper troposphere (not shown).

3.3 Atmospheric and oceanic anomalies associated with the north–south dipole mode EOF2

As for the north–south dipole mode (EOF2) of winter precipitation over SC, the linear regressions onto the PC2 show
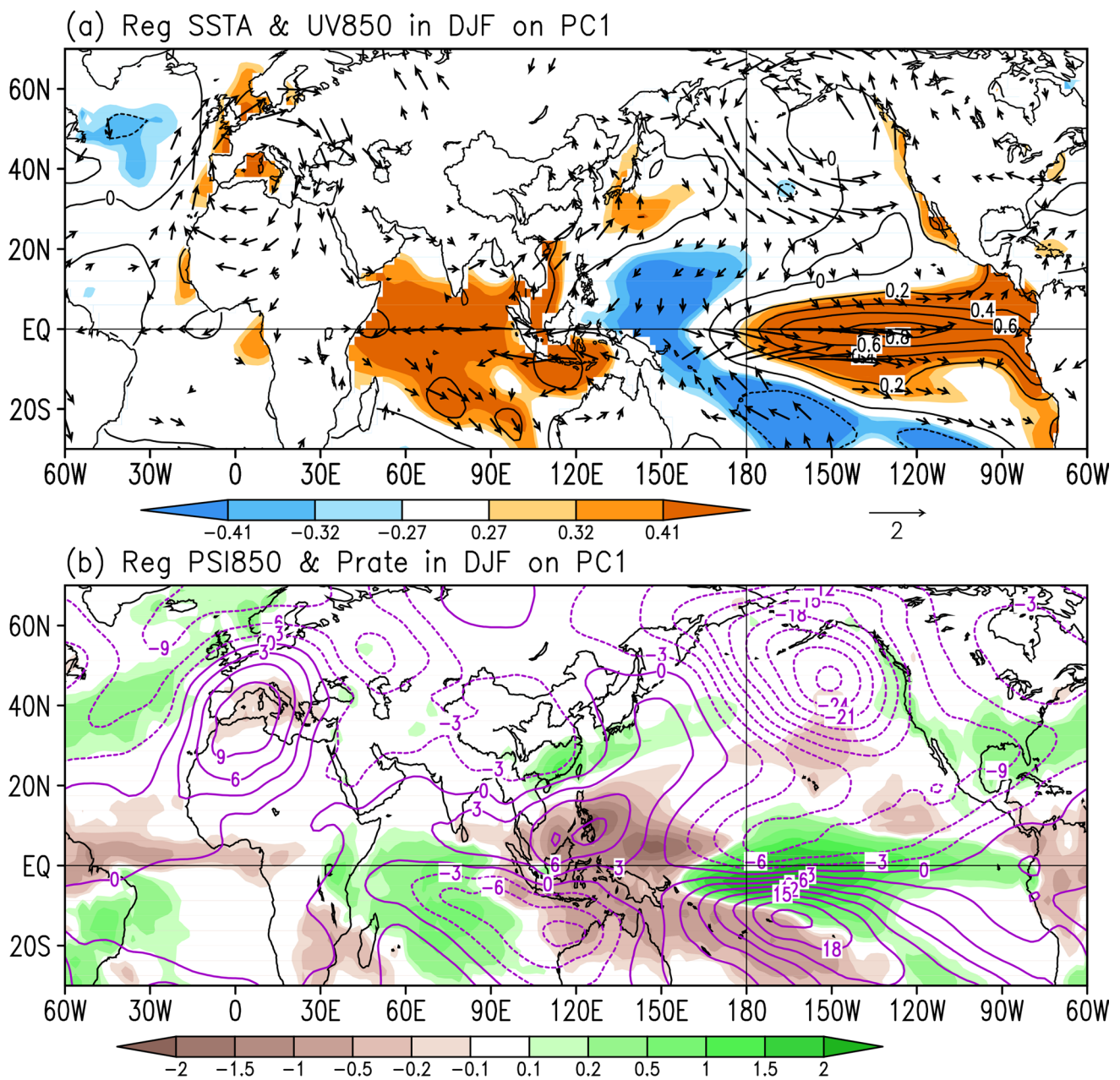
Fig. 2 Linear regressions onto the PC1. **a** SSTA (contour, °C) and 850 hPa horizontal wind anomalies (vector, m/s). Vectors indicate the regression of either zonal or/and meridional wind significant above 95% confidence level, and shadings from light to dark indicate the regression of SSTA significant above 90%, 95%, and 99% confidence levels, respectively. **b** 850 hPa eddy stream function (contour, interval: 3×10^5 m²s⁻¹) and precipitation (shading, mm/day) anomalies

that both the atmospheric circulation in the lower troposphere and SST signals are different from and weaker than those related to PC1 (Figs. 2a, 3a). Corresponding to positive PC2, there are positive SSTAs in the equatorial Atlantic Ocean (30°W–0°, 3°S–3°N) and a moderate SST cooling in the western Pacific warm pool (120°–140°E, 0°–10°N) (Fig. 3a). The cooling in the western Pacific warm pool is about 10 degrees westward compared with that associated with PC1 (Fig. 2a). Such the Pacific warm pool cooling

appears with the emergence of El Niño (Nitta and Hu 1996; Wang et al. 2000; Kug et al. 2009; Hu et al. 2012) and can be measured by the NiñoW index, which has significant negative correlations with all the ENSO-related indices used in this work, with the most negative correlation coefficient of -0.76 with the Modoki index (Table 2).

Previous studies indicated that the equatorial Atlantic SSTAs have a significant lag correlation with ENSO (Alexander and Scott 2002; Keenlyside and Latif 2007;

Table 2 Correlation coefficients among the leading PCs of winter precipitation over SC and various tropical SST indices during DJF 1981/82–2018/19 after the linear trends have been removed

SST index	Niño3.4	CT	WP	Modoki	NiñoW	IOBM	ATL3
PC1	**0.6****	**0.65****	0.1	0.17	− 0.31	**0.59****	0.01
PC2	0.05	− 0.02	0.24	0.18	**− 0.37***	0.15	**0.41****
Niño3.4		**0.9****	**0.59****	**0.63****	**− 0.62****	**0.76****	0.1
CT			0.19	0.23	**− 0.38***	**0.76****	0.2
WP				**0.97****	**− 0.69****	**0.34***	− 0.02
Modoki					**− 0.76****	**0.35***	− 0.12
NiñoW						**− 0.36***	0.08
IOBM							0.19

Superscript * and ** denote significance at 95% and 99% significance level using Student's t-test, corresponding to the absolute value of the correlation ≥ 0.32 and ≥ 0.41, respectively

Rodriguez-Fonseca et al. 2009; Hu et al. 2011). However, the simultaneous correlations between the ATL3 index (representing the equatorial Atlantic variation) and all the ENSO-related indices are not statistically significant (Table 2). It is implied that the simultaneous effect of ENSO on the Atlantic variability is weak. Chang et al. (2006) explained that this is because of the offset of the atmospheric response to the ENSO signal by the opposing influence of oceanic processes. Thus, the warming in the equatorial Atlantic Ocean and the cooling in the Pacific warm pool may be two independent potential contributors to the positive phase of the north–south dipole mode of the winter precipitation anomalies over SC. The above SSTA distribution is accompanied by anomalous westerly over the equatorial Atlantic, the northwestward shifted WNP anticyclone, and strong southerly surface wind anomalies over East China, which is favorable to water vapor convergence and more precipitation over LRYR in winter (Fig. 4b). Thus, the WNP anticyclone is a critical factor that bridges tropical oceanic anomaly and the winter precipitation variation, and its position determines the spatial distribution of the winter precipitation anomalies in SC.

The regressions of the precipitation and stream function anomalies onto PC2 show that the positive precipitation anomaly (heating) is seen in the equatorial central-western Atlantic Ocean, which is a response to the equatorial Atlantic SST warming (Fig. 3a). However, unlike the Pacific-East Asian teleconnection associated with the same-sign mode that primarily exists in the lower troposphere, the response to the equatorial Atlantic oceanic heating is strong in the tropical upper troposphere, with a pair of anticyclones (cyclones) symmetrical about the equator and centered at about 15°N and 15°S, respectively, and straddling the heating (cooling) pattern (Fig. 3b). This kind of tropical heating-atmospheric circulation response pattern is also present in the tropical Pacific (Fig. 3b). The precipitation anomalies in the tropical Pacific are also an east–west dipole structure, similar to the pattern associated with PC1, but much weaker and more westward.

Furthermore, the wave activity flux vectors in Fig. 3b, which represents the energy dispersion features associated with a Rossby wave train (Takaya and Nakamura 2001), indicate a remote influence of the equatorial Atlantic SSTAs on the East Asian climate through a Eurasian zonal wave train in the subtropical and mid-latitudes. Hu et al. (2018) found that the leading EOF mode of winter winds at the upper troposphere is a wave-like atmospheric teleconnection pattern along with the wintertime Asian jet. The wave train propagates northeastward from the North Atlantic to Europe, turns southeastward to the Middle East with amplifying amplitude, propagates along the jet to southern China, where an anomalous cyclonic center forms. The regressed stream function and wave activity flux anomalies on PC2 shows that the equatorial Atlantic warming modulates the Rossby wave train from the North Atlantic Ocean to East Asia in the mid-latitudes (Fig. 3b). A similar wave train originates from the tropical North Atlantic Ocean and propagates northeastward to the Arabian Peninsula, and then moves eastward via Tibetan Plateau to the eastern coast of China where an anomalous anticyclone forms in the upper-troposphere. As the atmospheric circulation anomalies in extratropics are quasi-barotropic (Wallace and Blackmon 1983), it is conducive to the northward shift of the WNP anticyclone. The local atmospheric circulation anomalies are accompanied by strong southerly low-level wind anomalies over East China, with the convergence of water vapor mainly in LRYR (Fig. 4b), thus forming a north–south dipole pattern of precipitation anomalies over SC.

The above analysis indicated that the positive same-sign pattern is related to the EP type El Niño and the tropical Indian warming, corresponding to a stronger and further southward anomalous WNP anticyclone. That leads to strong water vapor transport that mainly converges over the southeastern coast and east of China (Fig. 4a). The formation of the water vapor convergence belt north of around 15°N results in excessive precipitation in SC, with the largest center located on the southeast coast of China. The positive north–south dipole pattern, however,
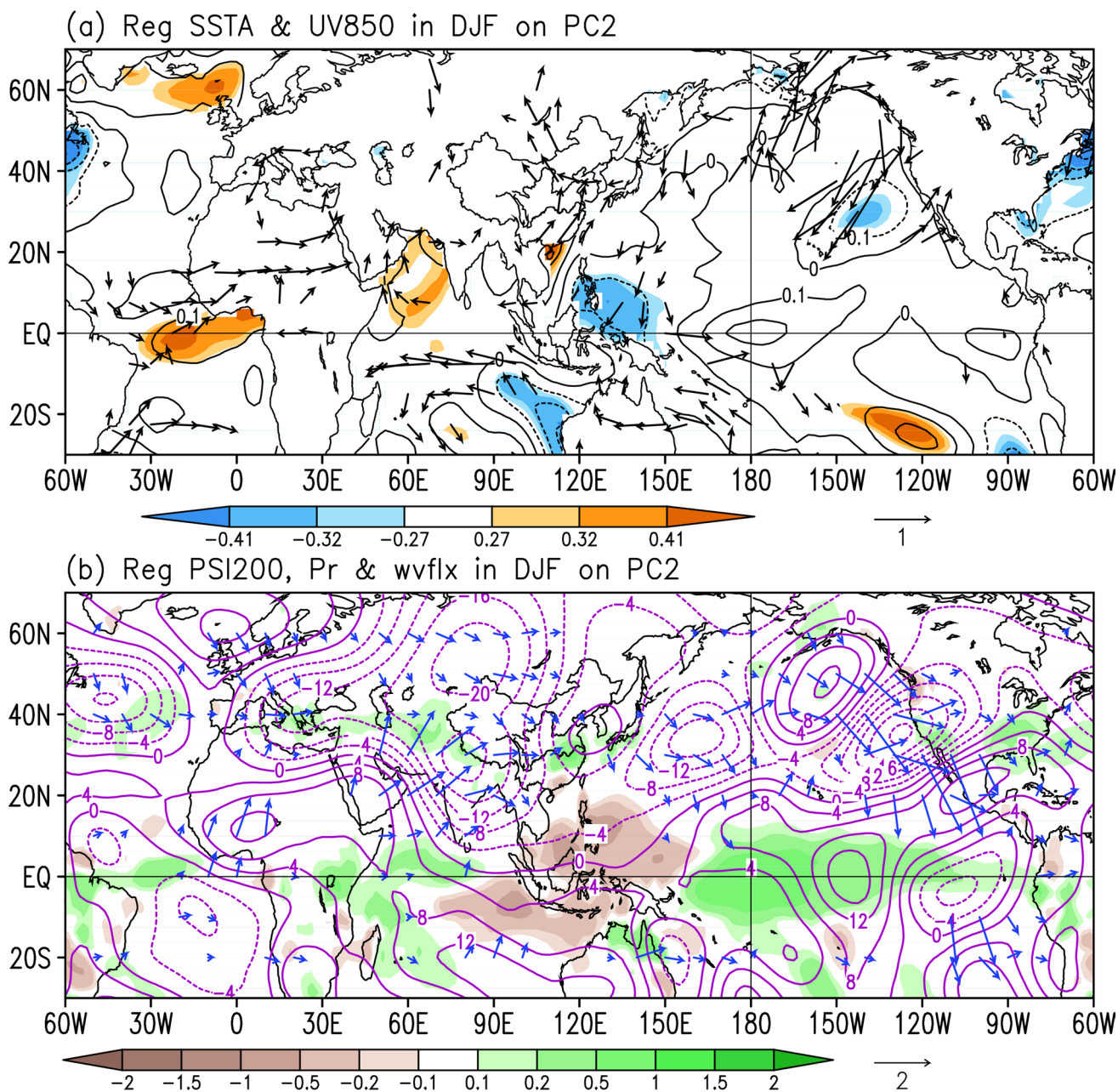
(a) Reg SSTA & UV850 in DJF on PC2

(b) Reg PSI200, Pr & wvflx in DJF on PC2

Fig. 3 Linear regressions onto the PC2. **a** SSTA (contour, °C) and 850 hPa horizontal wind anomalies (vector, m/s). Vectors indicate the regression of either zonal or/and meridional wind significant above 95% confidence level, and shadings from light to dark indicate the regression of SSTA significant above 90%, 95%, and 99% confidence levels, respectively. **b** Linear regression of 200 hPa eddy stream function (contour, interval: 5×10^5 m^{2}s^{-1}), precipitation (shading, mm/day), and wave activity flux (vectors, m^{2}s^{-2}) anomalies

is primarily affected by the western Pacific warm pool cooling and equatorial Atlantic warming, corresponding to a further northwestward anomalous WNP anticyclone compared with that of PC1. Thus, the water vapor transport is weaker and extends further north to the Yangtze River. LRYR is the water vapor convergence region which is located at the northwestern edge of the anomalous

anticyclone, while the southeastern coast of China is the moisture divergence region which is located at the southwestern edge of the anticyclone (Fig. 4b). Such distribution of the water vapor transport and associated convergence and divergence results in the north–south dipole mode of precipitation over SC, with weaker anomalies compared with the same-sign pattern.
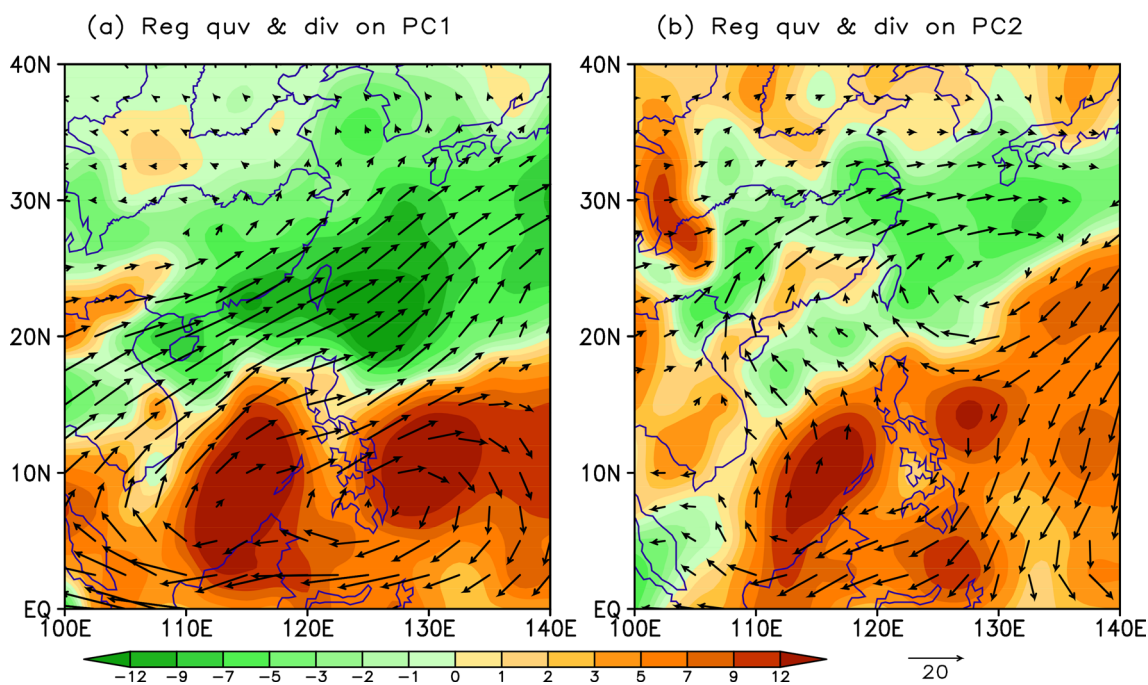
Fig. 4 Linear regressions of vertically integrated water vapor transport between surface and 300 hPa (vector, kg m^{-1} s^{-1}) and divergences (shading, 10^{-5} kg s^{-1} m^{-2}) on (**a**) PC1 and (**b**) PC2

4 Roles of the equatorial Atlantic and western Pacific

How do the SSTAs in the equatorial Atlantic and western Pacific warm pool work in the formation of the north–south dipole mode of winter precipitation over SC? To examine the SST influences in the above two regions, we use ATL3 and NiñoW indices to represent the SSTAs of the two regions, respectively. The year-to-year variations of the normalized ATL3 and NiñoW indices with the PC2 are given in Fig. 5. The simultaneous correlation is 0.41 between the ATL3 and PC2, and − 0.37 between the NiñoW and PC2. This suggests that the tropical Atlantic warming and the warm pool cooling favor excessive precipitation in the LRYR and deficit precipitation in the southeastern coast of China, the positive phase of the dipole-like variation.

The further detailed corresponding relationship between PC2 and ATL3 and NiñoW indices in the abnormal years of PC2 and the corresponding ATL3 and/or NiñoW indices if they are also abnormal years during the period from 1981/82 to 2018/19, are investigated based on the composite analysis. The criteria for an abnormal year are that the magnitudes of the normalized PC2 and the ATL3 and NiñoW indices exceed 0.5 standard deviations. Among a total of 11 abnormal years of PC2 and ATL3, there are 9 years (1991/92, 1995/96, 1996/97,1997/98, 2002/03, 2012/13, 2013/14, 2014/15, 2018/19) with a same-sign ATL3-PC2 relationship (including positive SST-positive PC2 and

negative SST-negative PC2 anomalies) and 2 years (1992/93, 2010/11) with an opposite-sign relationship (Fig. 5a). While for the abnormal years of PC2 and NiñoW, there are 8 years (1985/86, 1990/91, 1992/93, 1998/99, 2004/05, 2010/11, 2017/18, 2018/19) with an opposite-sign NiñoW-PC2 relationship and 1 year (1991/92) with a same-sign relationship (Fig. 5b). These corresponding relationships further confirm the robustness of the relation of PC2 with the ATL3 and NiñoW indices. In the following, we perform composite analyses based on the abnormal cases with a same-sign ATL3-PC2 relationship and with an opposite-sign NiñoW-PC2 relationship, respectively.

4.1 The ATL3 SST influence

Nine years with a same-sign ATL3-PC2 relationship are used in the composite (the mean of positive abnormal ATL3 years minus the mean of negative abnormal ATL3 years) analysis for the ATL3 cases in Fig. 6. During these years, basin-wide warming is observed in the tropical Atlantic Ocean, with the low-level anomalous westerly over the western Atlantic and anomalous easterly from the central Indian Ocean to the eastern Atlantic (Fig. 6a). The equatorial Atlantic warming induces an anomalous cyclone north of the equator, which is manifested by the equatorward flows associated with the equatorial westerly anomalies over the western Atlantic, with strong cyclonic vorticities. Also, an anomalous anticyclone appears to the east associated with

Fig. 5 Time series of the normalized PC2 of winter precipitation over SC (black line), and corresponding (**a**) the normalized detrend ATL3 or (**b**) NiñoW indices (red and blue bar) for the period of 1981/82–2018/19. Grey dashed lines are the criteria of the 0.5 standard deviations
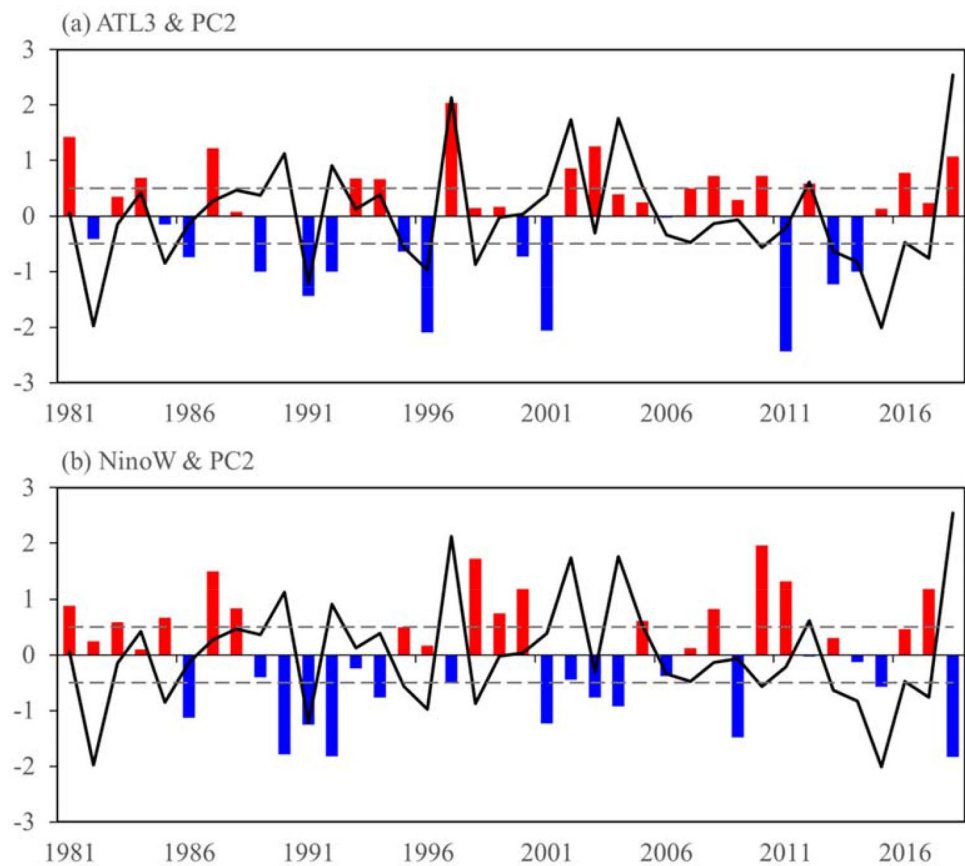
the equatorial anomalous easterly from the central Indian Ocean to the eastern Atlantic. The low-level southwesterly anomalies are located over SC (Fig. 6a). This kind of remote influence of the equatorial Atlantic on the winter East Asian atmospheric circulation anomalies seems to be through a zonal teleconnection in the upper troposphere (Fig. 6b). The corresponding stream function and wave activity flux vectors show a wave train from the tropical Atlantic to the midlatitudes of East Asia captured to some extent in the upper troposphere though there is a slight deviation in the position of anomalous centers compared with that of regressions onto PC2 (Fig. 3b). It originates from the tropical North Atlantic-western coast of Africa continent and propagates northeastward to western Asia-Tibetan Plateau, and then move eastward to East Asia. The anomalous anticyclone in the upper troposphere over East Asia is conducive to the northward shift of the WNP anticyclone and southerly wind over SC as the atmospheric circulation anomalies in extratropics are quasi-barotropic (Wallace and Blackmon 1983). It is also noted that the composite anomalies of stream function in Fig. 6b presents a meridional out-of-phase pattern of atmospheric circulation over the North Atlantic Ocean associated with the zonal teleconnection, which is consistent with Fig. 3b. This seems the pathway of the equatorial Atlantic SSTA influencing winter precipitation in SC. The similarity

of the composite tropical precipitation, S200, and associated WAF in the anomalous ATL3 winters to the regressions onto PC2 supports the effect of ATL3 warming by the wave train. It is implied that anomalous warming in the tropical Atlantic Ocean can generate anomalous circulation in the midlatitude region and induces precipitation anomaly over SC.

4.2 The NiñoW SST influence

Figure 7 presents the composite fields of 8 abnormal yeares with an opposite-sign NiñoW-PC2 relationship (the mean of negative abnormal NiñoW years minus the mean of positive abnormal NiñoW years). A CP El Niño-like pattern is shown in the composite fields (Fig. 7a). Significant negative SSTAs are observed in the warm pool, and significant positive SSTAs are observed in the equatorial central-eastern Pacific, accompanied by abnormal westerly anomaly over the equatorial central Pacific and anomalous WNP anticyclone (Fig. 7a). This is similar to the SST and low-level wind anomaly field associated with PC1 (Fig. 2a), but the SSTA center and the corresponding westerly anomaly, as well as the position of the Philippine anticyclone, are further westward than the latter ones. Moreover, the low-level stream function and precipitation also show the response of the CP-El Niño-like warming.

(a) Composite SSTA & UV850 of abnormal ATL3 winter
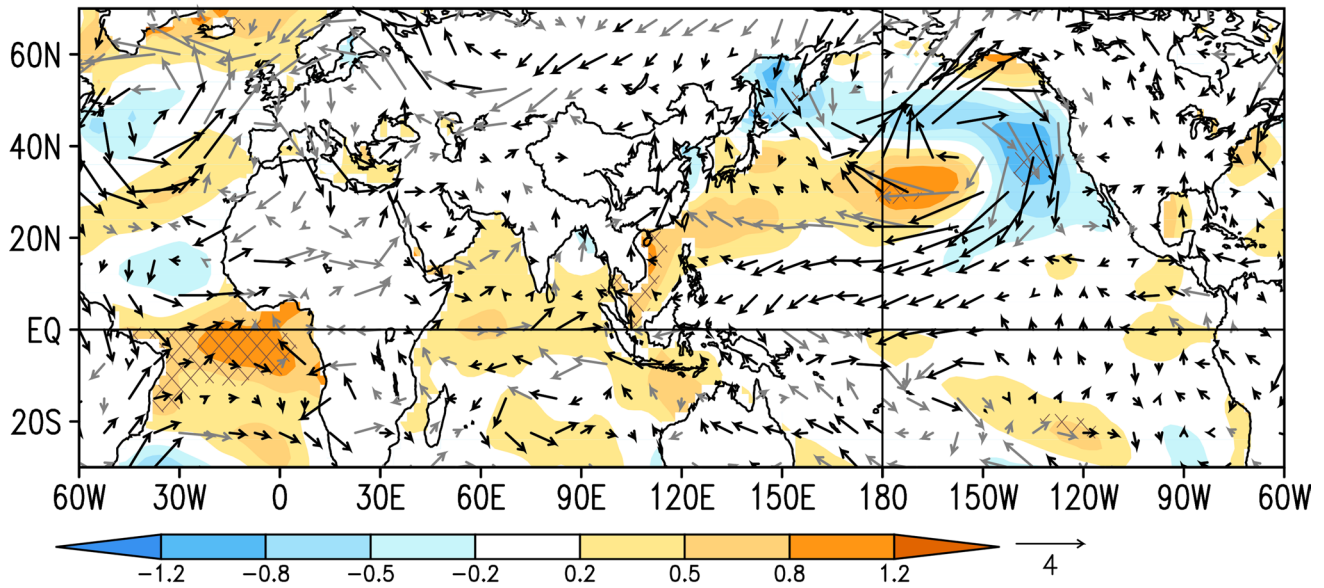
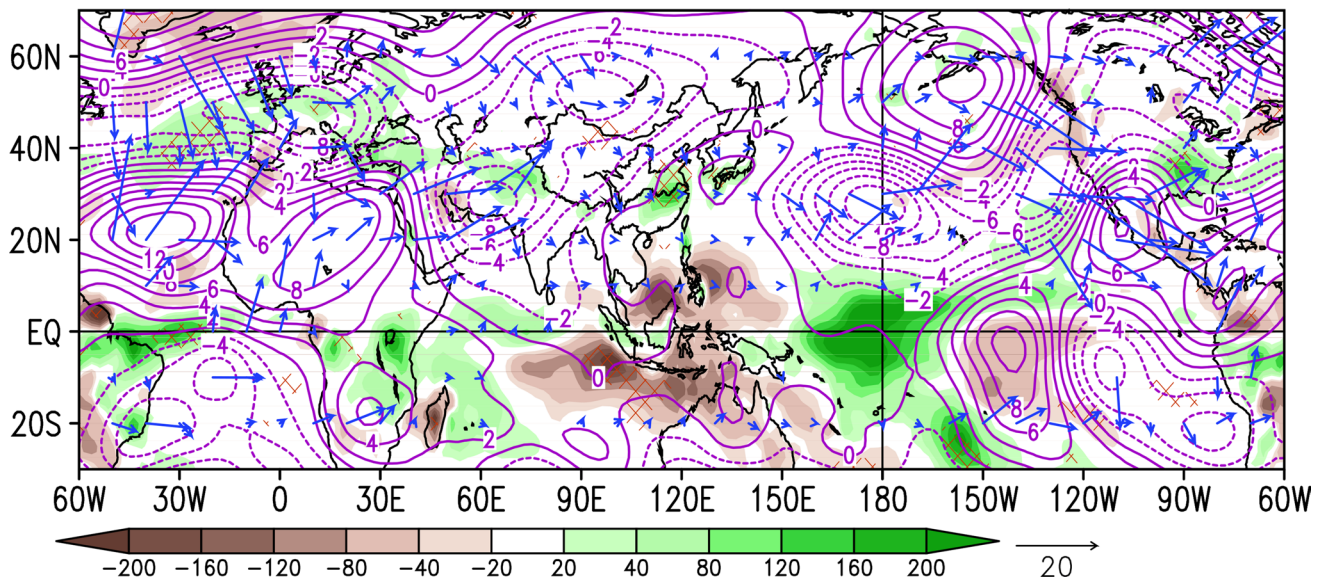## (b) Composite PSI200, Prate & wvflx of abnormal ATL3 winter

Fig. 6 Composite anomalies for the ATL3 cases of (**a**) SST (shading, ℃) and 850 hPa wind (vector, m·s^{-1}; thick vectors exceed 95% confidence level for either u or/and v components); (**b**) precipitation (shading, mm), 200 hPa eddy st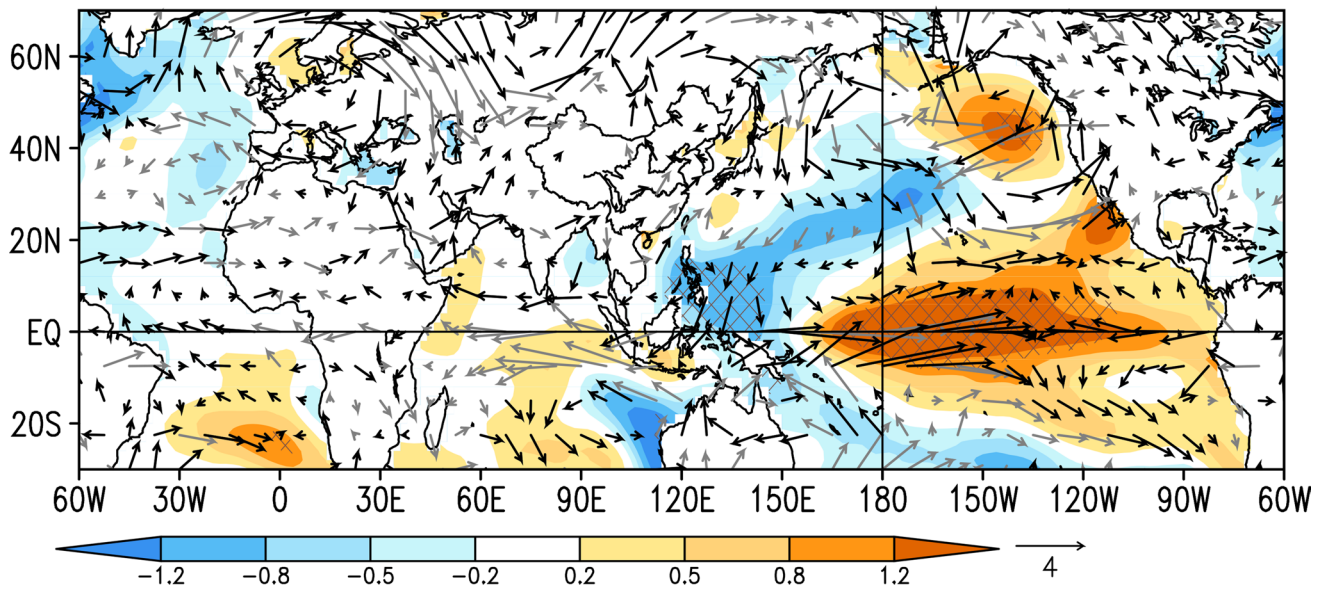ream function (contour, interval: 2×10^5 m^{2}s^{-1}) and wave activity flux (vectors, m^{2}s^{-2}). The hatched regions in indicate that the composite of SSTAs in (**a**) and precipitation in (**b**) are statistically significant at 99% confidence level

An east–west dipole structure of precipitation anomalies in the tropical Pacific, and the antisymmetric anomalous stream function pattern about the equator feature a Rossby wave response to anomalous heating over the equatorial central Pacific (Gill 1980; Alexander et al. 2002). Due to the westward shift of the warm pool cooling, it is favorable to the enhancement of the anomalous anticyclone over SCS, the northward extension of the WNP anticyclone,

and further northward water vapor transport with convergence over the LRYR.

Overall, the equatorial Atlantic warming causes strong southerly anomaly over SC through a zonal wave pattern in the upper troposphere, and the western Pacific warm pool cooling induces the westward shift of SCS-Philippine anticyclone through the lower-tropospheric central Pacific-East Asian teleconnection. Both the ATL3 warming and

(a) Composite SSTA & UV850 of abnormal NinoW winter

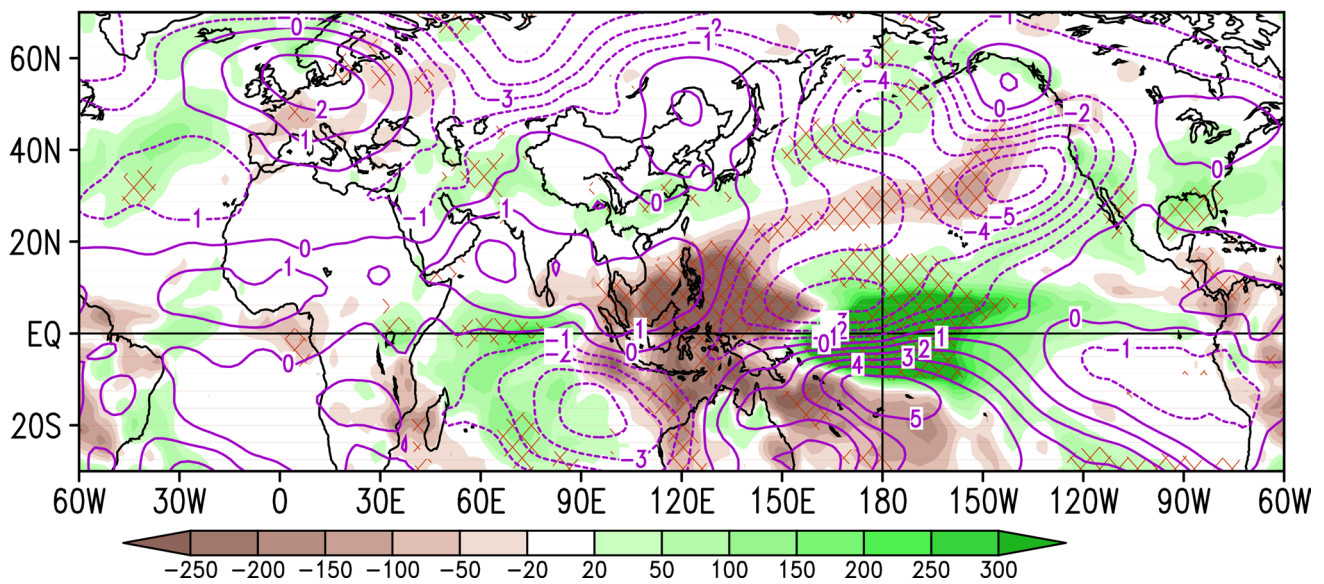## (b) Composite PSI850 & Prate of abnormal NinoW winter

Fig. 7 Composite anomalies for the NiñoW cases of (**a**) SST (shading, ℃) and 850 hPa wind (vector, m·s^{-1}; thick vectors exceed 95% confidence level for either u or/and v components); (**b**) precipitation (shading, mm) and 850 hPa eddy stream function (contour, interval: 2 $\times 10^5$ m^{2}s^{-1}). The hatched regions indicate that the composite anomalies of SST in (**a**) and precipitation in (**b**) are statistically significant at 99% confidence level

NiñoW cooling coherently lead to the northwestward shift of the WNP anticyclone, resulting in a dipole–like variation pattern of winter precipitation over SC with positive anomalies in the north and negative anomalies in the south. Besides, the composite of the extreme ATL3-PC2 cases (1991/92, 1996/97, 1997/1998, 2018/2019) and extreme NiñoW-PC2 cases (1990/91, 1992/93, 2018/19)

with the criteria of one standard deviation have consistent results (Figure not shown).

5 CFSv2 predictions

The predictability and possible connection of SSTAs with the SC winter precipitation variability is further examined
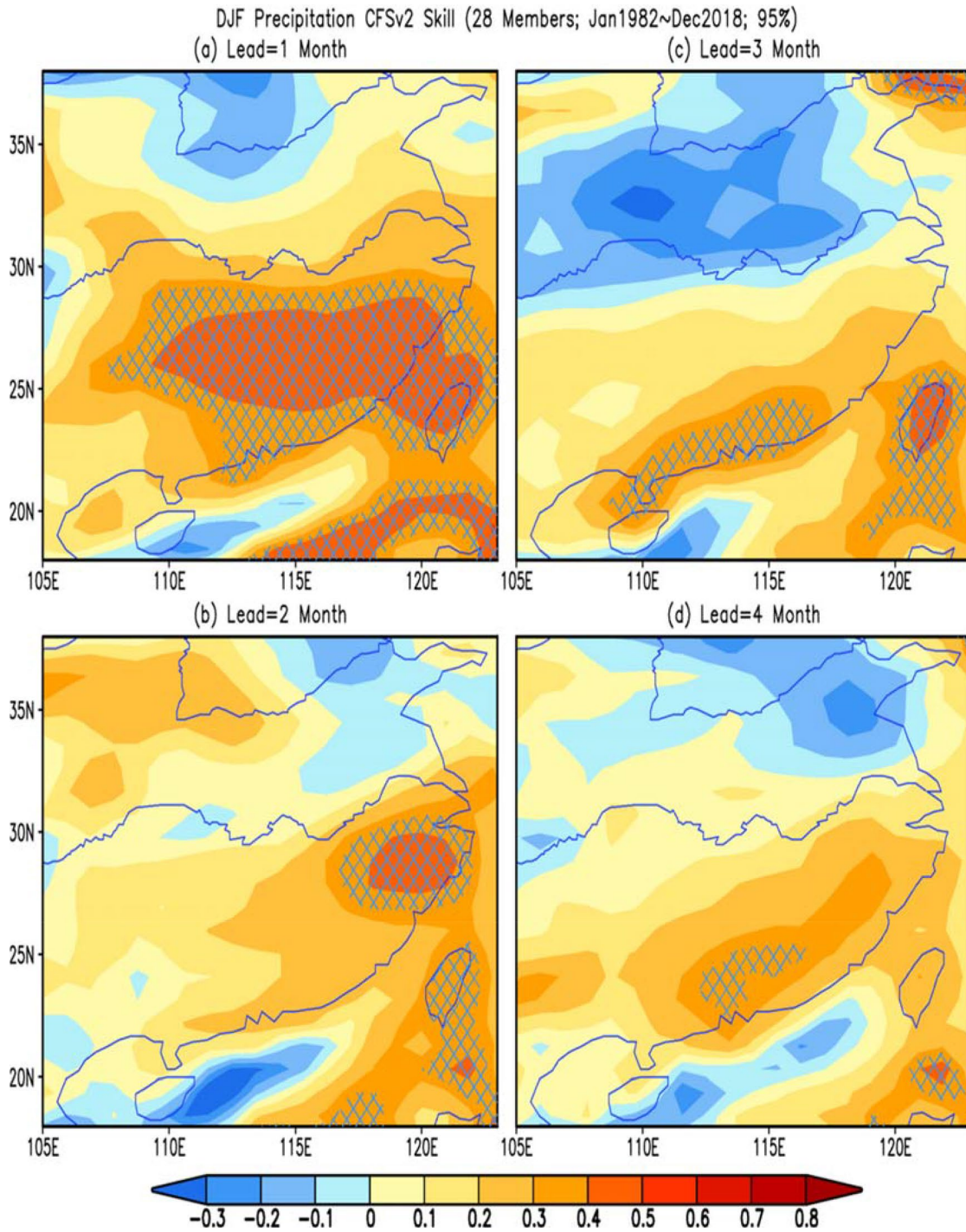

Fig. 8 Correlations of the observed and CFSv2 predicted DJF precipitation anomalies with lead time of (**a**) 1-month, (**b**) 2-month, (**c**) 3-month, and (**d**) 4-month during 1982–2018. The hatched regions represent the correlations significant above 95% confidence level according to Student's *t*-test

by model predictions. The NCEP CFSv2 model is selected which shows a good prediction skill for the SC winter precipitation in 1–4 month leads during DJF 1982/83–2017/18 (Fig. 8). It is noted that the highest prediction skill of winter precipitation variability within the displayed region is in the south of the middle and low reaches of the Yangtze River. The skillful predictions in the 1–4 month leads are beyond the predictability of the atmospheric internal dynamical process, thus, it implies that boundary forcing, such as SST forcing, must play a role in the winter precipitation variation in SC. That is consistent with the statistical connections of SSTAs in the tropical Pacific and Atlantic Oceans with winter climate variability discussed in previous subsections.

For the impact of SSTAs in the tropical Pacific on winter precipitation in SC, there have been well-documented mechanisms (Wu et al. 2003; Feng et al. 2010; Hu et al. 2012; Su et al. 2013). Thus, here, we focus on the connection between the equatorial Atlantic warming and the north–south dipole mode of SC winter precipitation. The two regional mean precipitation anomaly difference between LRYR (28°–31°N, 114°–122°E) and southeast coast of China (22°–25°N, 110°–117°E) is used to represent the north–south dipole-like variation, and the model's performance for the north–south dipole-like variation corresponding to different lead times are shown in Fig. 9. A comparison of the predictions at different leading times shows that the characteristics of the dipole mode are captured to some extent in the short lead predictions. The correlation coefficients of the observed dipole index with the CFSv2 predicted ones in 0-, 1-, and 2-month leads are 0.32, 0.36, 0.38, respectively. On the other hand, Liu et al. (2020) indicated that the observed SSTAs in the tropical oceans are well captured in the short lead predictions (Fig. 12 in Liu et al. 2020), and the prediction ability of SST in the CFSv2 model is crucial for the predictability of precipitation in East Asia.

Figure 10 shows the relationship of the north–south dipole mode with the ATL3 index corresponding to different lead times. It is noted that there are significant correlations between the SC winter precipitation variability and the ATL3 index during 37 winters of 1982/83–2017/18 in CFSv2, with the correlation coefficients of 0.52 ~ 0.31 in the 1 ~ 4 month leads. The model skillful forecast results are a support for the possible connection between boundary founding (the equatorial Atlantic and western Pacific SSTA) and the north–south dipole-like variation of SC winter precipitation in the observations (Fig. 3).

5.1 Conclusions and discussion

In this work, the two leading modes of the winter precipitation over SC are identified first, and the contributions of tropical oceanic forcing are further investigated to address the possible impact of equatorial Pacific and Atlantic

SSTAs on the leading modes and the mechanisms. The two leading modes of the winter precipitation anomaly over SC are the same-sign mode (EOF1) with the maximum center located on southeastern China, and the south-north dipole mode with the opposite variations (EOF2) between LRYR and the southeastern coast of China, respectively.

The key system that bridges both the tropical Pacific and Atlantic Oceanic forcing and the winter precipitation anomalies over SC is an anomalous anticyclone located in the WNP at the lower troposphere. For the same-sign mode (EOF1), it is mainly associated with canonical El Niño which influences the anticyclone through the Pacific-East Asian teleconnection. In the positive phase of the north–south dipole mode (EOF2) with above-normal precipitation in the north and blow-normal in the south, in addition to the impact from the Pacific warm pool associated with CP El Niño, the impact of tropical Atlantic warming is through altering the winter Atlantic-Eurasian atmospheric circulation via a zonal wave pattern in the mid-latitudes originating from the tropical Atlantic and propagating northeastward to East Asia. Both the tropical Pacific and Atlantic Oceanic forcing affect the northward extension of the WNP anticyclone, with a further northward extension of water vapor transport to the Yangtze River. LRYR is the water vapor convergence region which is located at the northwestern edge of the anomalous anticyclone while the southeastern coast of China is the moisture divergence region, resulting in a north–south dipole mode of winter precipitation anomaly over SC. Furthermore, the relationship between the dipole-like variation of the winter precipitation in SC and the equatorial Atlantic SSTA in the CFSv2 is consistent with that in the observations, which is a support for the observed statistical relationship between them.

The novel part of this work is that it is the first time indicating the impact of the equatorial Atlantic Ocean on the dipole-like variation of winter precipitation in South China. However, the SSTA amplitude in the equatorial Atlantic is statistically smaller than that in the equatorial Pacific, which may potentially result in a smaller variability of the atmospheric circulation anomalies. Also, the analyses using raw data (without removing the linear trend) or adopting 9-year high pass filter for all the variables (figures not shown) lead to consistent results, indicating that interannual variation of SSTA in the tropical Pacific and Atlantic Oceans is potentially a major source of the winter precipitation variability and predictability in SC. However, the influence of the tropical Atlantic Ocean on winter climate in South China may experience interdecadal variation (Park et al. 2019). That deserves further investigation with long observational data and model simulation, and the diagnosis results in this work need to be verified by designed sensitivity experiments and theoretical studies.
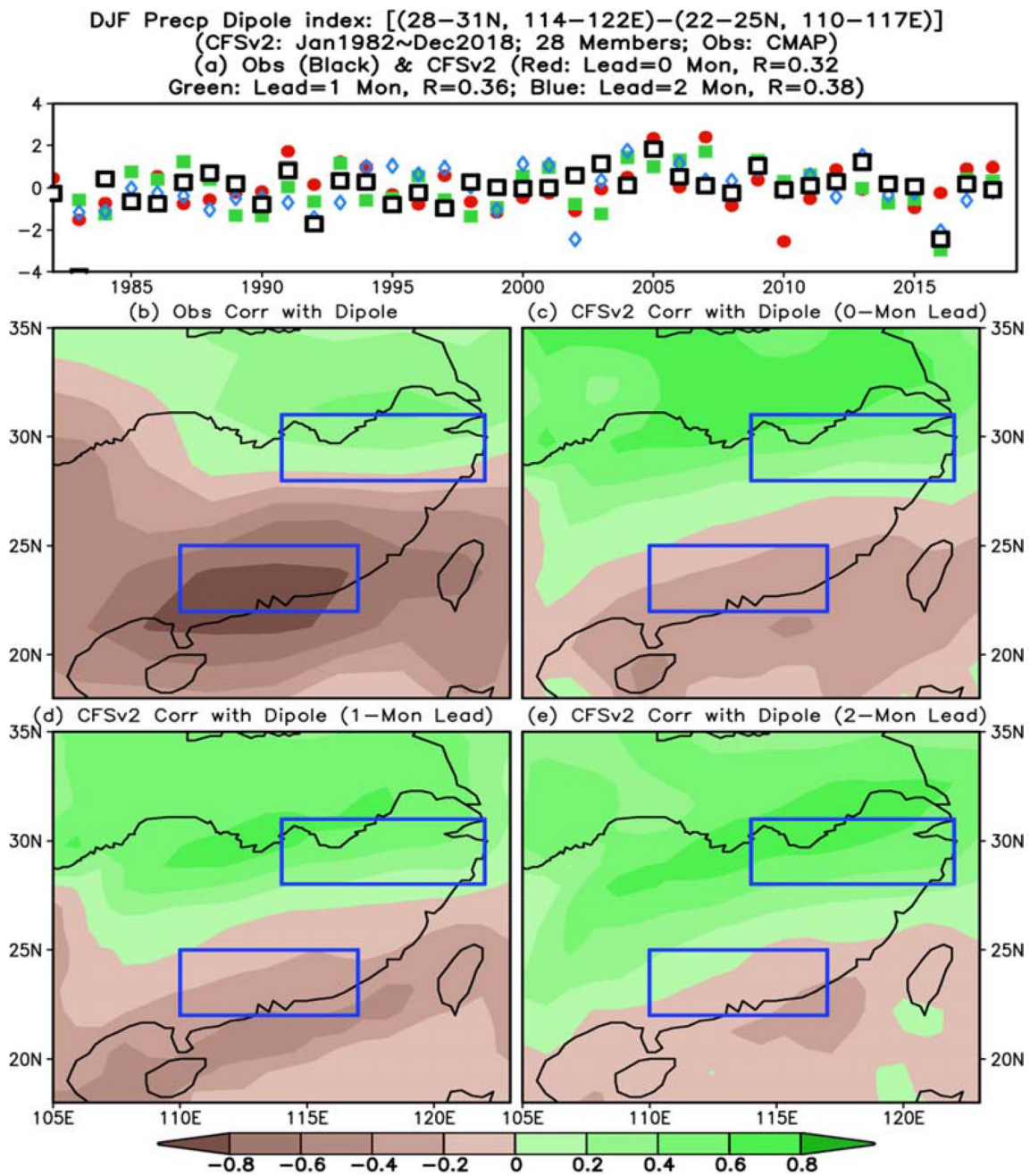
Fig. 9 a The dipole index of precipitation in DJF in the observation (black square); in the ensemble mean of CFSv2 predictions with the lead times of 0 (closed red circle), 1 (closed green square), and 2 (open blue diamond) months; Correlations of the dipole index with precipitation in DJF in (**b**) observations; CFSv2 predictions of 0 (**c**), 1 (**d**), 2 (**e**) month lead. The correlation coefficients of the observed dipole index with the CFSv2 predicted ones in 0-, 1-, and 2-month leads are 0.32, 0.36, 0.38, respectively. Here the dipole index is referred to as the differences of the averaged precipitation between the north (28°–31ºN, 114°–122ºE) and south (22°–25ºN, 110°–117ºE) (see the blue rectangles in (**b–e**)
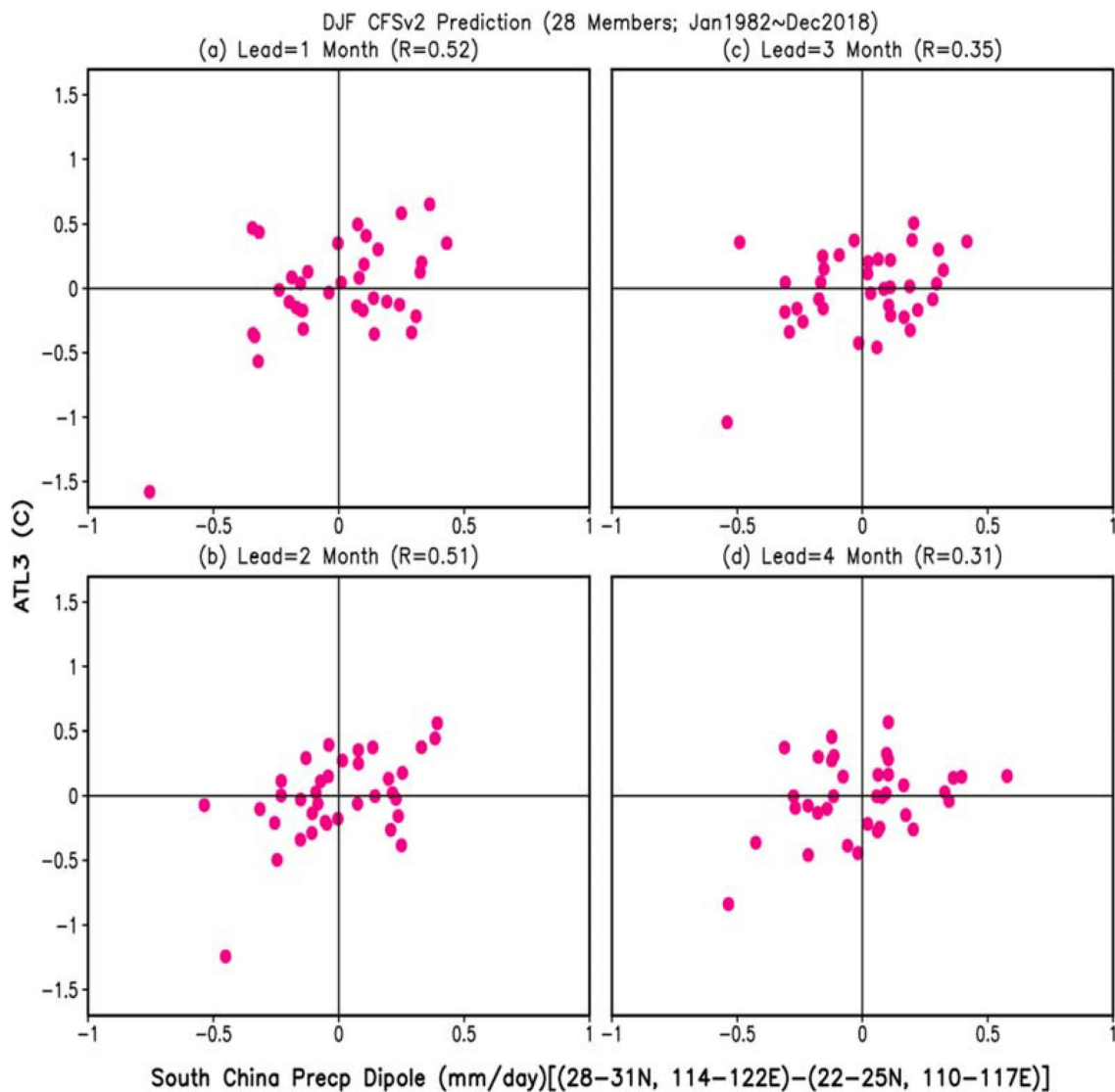
Fig. 10 Scatter plot of the north–south dipole mode of SC precipitation (x-axis, mm/day) vs the ATL3 index (y-axis, °C) in the (**a**) 1-month, (**b**) 2-month, (**c**) 3-month, and (**d**) 4-month leads in CFSv2 predictions in 1982–2018. The correlation coefficients (R) between them are shown at the top of each panel

References

Alexander M, Blade I, Newman M, Lanzante J, Lau N-C, Scott J (2002) The atmospheric bridge: the influence of ENSO teleconnection on air-sea interaction over the global oceans. J Clim 15:2205–2231

Alexander M, Scott J (2002) The influence of ENSO on air-sea interaction in the Atlantic. Geophys Res Lett 29:1701. https://doi.org/10.1029/2001GL014347

Ashok K, Behera SK, Rao SA, Weng H, Yamagata T (2007) El Niño Modoki and its possible teleconnection. J Geophys Res 112:C11007. https://doi.org/10.1029/2006JC003798

Chambers DP, Tapley BD, Stewart RH (1999) Anomalous warming in the Indian Ocean coincident with El Niño. J Geophys Res 104:3035–3047

Chang P, Fang Y, Saravanan R, Ji L, Seidel H (2006) The cause of the fragile relationship between the Pacific El Niño and the Atlantic Niño. Nature 443:324–328. https://doi.org/10.1038/nature05053

Chang CP, Wang Z, Ju JH, Li T (2004) On the relationship between western maritime continent monsoon rainfall and ENSO during northern winter. J Clim 17:665–672. https://doi.org/10.1175/1520-0442(2004)017<0665:OTRBWM>2.0.CO;2

Chen M, Xie P, Janowiak JE, Arkin PA (2002) Global land precipitation: A 50-years monthly analysis based on gauge observations. J Hydrometeorol 3:249–266

Chen W, Lee JY, Lu R, Dong B, Ha KJ (2015) Intensified impact of tropical Atlantic SST on the western North Pacific summer climate under a weakened Atlantic thermohaline circulation. Clim Dyn 45:2033–2046. https://doi.org/10.1007/s00382-014-2454-4

Feng J, Wang L, Chen W, Fong SK, Leong KC (2010) Different impacts of two types of Pacific Ocean warming on Southeast Asian rainfall during boreal winter. J Geophys Res 115:D24122. https://doi.org/10.1029/2010JD014761

Fu J, Li S, Wang Y (2008) Influence of prior thermal state of global oceans on the formation of the disastrous snowstorm in January 2008. Clim Environ Res 13(4):478–490 (in Chinese)

Gill A (1980) Some simple solutions for heating-induced tropical circulation. Q J R Meteorol S 106:447–462

Guo L, Liu B, Zhu C (2019) Extraordinary long wet spell in south of Yangtze River during 2018/2019 winter and its possible causes. Chin Sci Bull 64:3498–3509. https://doi.org/10.1360/N9720 19-00357.(inChinese)

Guo Y, Ni Y (1998) Effects of the tropical Pacific convective activities on China's winter monsoon. Meteorology 24(9):3–7 (in Chinese)

Han Z, Li S, Mu M (2011) The role of warm North Atlantic SST in the formation of position of positive height anomalies over the Ural Mountains during January 2008. Adv Atmos Sci 28(2):246–256

He S, Wang HJ (2013) Oscillating relationship between the East Asian winter monsoon and ENSO. J Clim 26:9819–9838. https://doi.org/10.1175/jcli-d-13-00174.1

He Z, Wu R (2014) Indo-Pacific remote forcing in summer rainfall variability over the South China Sea. Clim Dyn 42:2323–2337. https://doi.org/10.1007/s00382-014-2123-7

Hu KM, Huang G, Wu RG, Wang L (2018) Structure and dynamics of a wave train along the wintertime Asian jet and its impact on East Asian climate. Clim Dyn 51:4123–4137

Hu Z-Z, Kumar A, Huang B, Xue Y, Wang W, Jha B (2011) Persistent atmospheric and oceanic anomalies in the North Atlantic from Summer 2009 to Summer 2010. J Climate 24(22):5812–5830. https://doi.org/10.1175/2011JCLI4213.1

Hu Z-Z, Kumar A, Jha B, Wang W, Huang BH, Huang BY (2012) An analysis of warm pool and cold tongue El Niños: air-sea coupling processes, global influences, and recent trends. Clim Dyn 38:2017–2035. https://doi.org/10.1007/s00382-011-1224-9

Hu Z-Z, Kumar A, Huang BH, Wang WQ, Zhu JS, Wen C (2013) Prediction skill of monthly SST in the North Atlantic ocean in NCEP climate forecast system version 2. Clim Dyn 40:2745–2756. https://doi.org/10.1007/s00382-012-1431-z

Hu Z-Z, Kumar A, Huang BH, Zhu JS, Guan Y (2014) Prediction skill of north pacific variability in NCEP climate forecast system version 2: impact of ENSO and beyond. J Clim 27:4263–4272. https://doi.org/10.1175/JCLI-D-13-00633.1

Hu Z-Z, Kumar A, Jha B, Zhu JS, Huang BH (2017) Persistence and predictions of the remarkable warm anomaly in the northeastern Pacific Ocean during 2014–2016. J Clim 30:689–702. https://doi.org/10.1175/JCLI-D-16-0348.1

Huang B, Thorne PW, Banzon VF, Boyer T, Zhang HM (2017) Extended Reconstructed sea surface temperature version 5 (ERSSTv5), upgrades, validations, and intercomparisons. J Clim 30:8179–8205. https://doi.org/10.1175/JCLI-D-16-0836.1

Huo L, Guo P, Saji H, Jin D (2015) The role of tropical Atlantic SST anomalies in modulating western North Pacific tropical cyclone genesis. Geophys Res Lett 42:2378–2384. https://doi.org/10.1002/2015GL063184

Jang H-Y, Yeh S-W, Chang E-C, Kim B-M (2016) Evidence of the observed change in the atmosphere-ocean interactions over the South China Sea during summer in a regional climate model. Meteorol Atmos Phys 128:639–648

Jin D, Hameed SN, Huo L (2016) Recent changes in ENSO teleconnection over the western pacific impacts the eastern china precipitation dipole. J Clim 29:7587–7598

Kalnay E, Kanamitsu M, Kistler R et al (1996) The NCEP/NCAR 40-Year Reanalysis Project. Bull Amer Meteor Soc 77:437–472

Ke Z, Jiang X, Wang Z (2019) Southeast China Boreal Winter Precipitation anomalies are dependent on intensity of El Niño. Sci Rep 9:17410. https://doi.org/10.1038/s41598-019-53496-5

Keenlyside NS, Latif M (2007) Understanding equatorial Atlantic interannual variability. J Clim 20:131–142. https://doi.org/10.1175/JCLI3992.1

Kug JS, Jin FF, An SI (2009) Two types of El Niño events: cold tongue El Niño and warm pool El Niño. J Clim 22:1499–1515. https://doi.org/10.1175/2008jcli2624.1

Lau N-C, Nath MJ (2003) Atmosphere-Ocean variations in the Indo-Pacific sector during ENSO episodes. J Clim 16:3–20. https://doi.org/10.1175/15200442(2003)016<0003:AOVITI>2.0.CO;2

Li S, Bates GT (2007) Influence of the Atlantic multi-decadal oscillation on the winter climate of East China. Adv Atmos Sci 24(1):126–135

Liu S, Bueh C, Tao S, Sui B (2010) A study of the statistical prediction method of the East Asian winter monsoon intensity. Chin J Atmos Sci 34(1):35–44 (in Chinese)

Liu Y, Ding Y, Gao H, Li W (2013) Tropospheric biennial oscillation of the western Pacific subtropical high and its relationships with the tropical SST and atmospheric circulation anomalies. Chin Sci Bull 58:3664–3672. https://doi.org/10.1007/s11434-013-5854-7

Liu Y, Hu Z-Z, Wu R (2020) Was the extremely wet winter of 2018/19 in the lower reach of the Yangtze River driven by ENSO? Int J Climatol. https://doi.org/10.1002/joc.6591

Nitta T, Hu Z-Z (1996) Summer climate variability in China and its association with 500 hPa height and tropical convection. J Meteor Soc Japan 74(4):425–445. https://doi.org/10.2151/jmsj1965.74.4_425

North GR, Bell TL, Cahalan RF, Moeng FJ (1982) Sampling errors in the estimation of empirical orthogonal functions. Mon Wea Rev 110(7):699–706

Park J-H, Li T, Yeh S-W, Kim H (2019) Effect of recent Atlantic warming in strengthening Atlantic-Pacific teleconnection on interannual timescale via enhanced connection with the Pacific meridional mode. Clim Dyn 53(1–2):371–387. https://doi.org/10.1007/s00382-018-4591-7

Peng P, Kumar A, Chen M, Hu Z-Z, Jha B (2019) Was the North American extreme climate in winter 2013/14 a SST forced response? Clim Dyn 52:3099–3110. https://doi.org/10.1007/s00382-018-4314-0

Ren H, Jin F-F (2011) Niño indices for two types of ENSO. Geophys Res Lett 38:L04704. https://doi.org/10.1029/2010GL046031

Rodriguez-Fonseca B, Polo I, Garcia-Serrano J, Losada L, Mohino E, Mechoso CR, Kucharski F (2009) Are Atlantic Niños enhancing Pacific ENSO events in recent decades? Geophys Res Lett 36:L20705. https://doi.org/10.1029/2009GL040048

Saha S et al (2014) The NCEP climate forecast system version 2. J Clim 27:2185–2208. https://doi.org/10.1175/JCLI-D-12-00823.1

Su JZ, Zhang RH, Zhu CW (2013) ECHAM5-simulated impacts of two types of El Niño on the winter precipitation anomalies in South China. Atmos Oceanic Sci Lett 6:360–364. https://doi.org/10.3878/j.issn.1674-2834.13.0013

Takaya K, Nakamura H (2001) A formulation of a phase independent wave activity flux for stationary and migratory quasigeostrophic eddies on a zonally varying basic flow. J Atmos Sci 58:608–627

Wallace M, Blackmon M (1983) Observations of low-frequency atmospheric variability. Academic Press, Large-Scale Dyn Proc Atmos, p p397

Wang B, Wu RG, Fu XH (2000) Pacific-East Asian teleconnection: How does ENSO affect East Asian climate? J Clim 13:1517–1536. https://doi.org/10.1175/1520-0442(2000)013<1517:PEATH D>2.0.CO;2

Wang H, Kumar A, Murtugudde R, Narapusetty B, Seip KL (2019) Covariations between the Indian Ocean dipole and ENSO: a modeling study. Clim Dyn 53:5743–5761. https://doi.org/10.1007/s00382-019-04895-x

Wu RG, Hu Z-Z, Kirtman BP (2003) Evolution of ENSO-related rainfall anomalies in East Asia. J Clim 16:3742–3758. https://doi.org/10.1175/1520-0442(2003)016<3742:EOERAI>2.0.CO;2

Xie SP, Hu K, Hafner J, Tokinaga H, Du Y, Huang G, Sampe T (2009) Indian Ocean capacitor effect on Indo-Western Pacific climate during the summer following El Niño. J Clim 22:730–747. https://doi.org/10.1175/2008jcli2544.1

Xu K, Huang QL, Tam CY, Wang WQ, Chen S, Zhu CW (2019) Roles of tropical SST patterns during two types of ENSO in modulating wintertime rainfall over southern China. Clim Dyn 52:523–538. https://doi.org/10.1007/s00382-018-4170-y

Xue Y, Chen M, Kumar A, Hu Z-Z, Wang W (2013) Prediction skill and bias of tropical Pacific sea surface temperatures in the NCEP Climate Forecast System version 2. J Clim 26:5358–5378. https://doi.org/10.1175/JCLI-D-12-00600.1

Yuan Y, Yang S (2012) Impacts of different types of El Niño on the East Asian climate: Focus on ENSO cycles. J Clim 25:7702–7722

Zebiak SE (1993) Air-sea interaction in the equatorial Atlantic region. J Clim 6:1567–1586. https://doi.org/10.1175/1520-0442(1993)006<1567:AIITEA>2.0.CO;2

Zhang RH, Sumi A, Kimoto M (1999) A diagnostic study of the impact of El Niño on the precipitation in China. Adv Atmos Sci 16:229–241

Zhang RH, Sumi A (2002) Moisture circulation over East Asia during El Niño episode in the northern winter, spring and autumn. J Meteor Soc Japan 80:213–227

Zhang Z, Gong D, Guo D, He X, Lei Y (2008) Anomalous winter temperature and precipitation events in southern China. Acta Geograph Sinica 63(9):899–912 **(in Chinese)**

Zong H, Zhang Q, Bueh C, Ji L, Chen L (2008) Numerical simulation of possible impacts of Kuroshio and North Atlantic sea surface temperature anomalies on the South China snow disaster in January 2008. Clim Environ Res 13(4):491–499 **(in Chinese)**